Ocean Dynamics (2021) 71:475–489
https://doi.org/10.1007/s10236-021-01444-1

Seasonal oceanic variability on meso- and submesoscales: a turbulence perspective

Boris Galperin[1] · **Semion Sukoriansky**[2] · **Bo Qiu**[3]

Received: 20 December 2019 / Accepted: 1 February 2021 / Published online: 8 March 2021

Abstract
Seasonal variability of the upper ocean on meso- and submesoscales is investigated in the framework of the quasi-normal scale elimination theory, or QNSE. The longitudinal and transverse velocity spectra in this theory have a bi-component structure comprised of the Coriolis and Kolmogorov-like branches that are identified with meso- and submesoscales, respectively. For the former, spectral amplitudes are determined by the Coriolis parameter, f, while for the latter, the amplitudes are quantified in terms of the energy flux, Π_ε, proceeding from larger to smaller scales. This flux can be identified with the *effective submesoscale dissipation*. The Kolmogorov and Coriolis subranges are delineated at a length scale L_c that marks a crossover between the respective spectra. The theoretical spectra agree well with those obtained in many observational campaigns. In phase with the seasonal variations of the intensities of instabilities and turbulence, the magnitudes of Π_ε and L_c increase in winter and decrease in summer. Mirroring these changes, the bi-component structure of the kinetic energy spectra changes with seasons and renders meaningless the characterization of their seasonal variability in terms of a single slope. The theoretical results are validated against the data collected in Oleander, LatMix and North-Western Pacific observations.

Keywords 92.10.ak Eddies and mesoscale processes · 92.10.Ei Coriolis effects · 92.10.Lq Turbulence, diffusion, and mixing processes in oceanography

1 Introduction

Oceanic submesoscale motions (SMMs) occupy the range of the horizontal scales from, approximately, $O(10^2)$ to $O(10^5)$ meters and vertical scales in the range of $O(10)$ to $O(10^2)$ meters (McWilliams 2019). In the taxonomy of the scales of Oceanic General Circulation shown in Fig. 1 in McWilliams (2019), the SMMs are placed in the range between the balanced instabilities and turbulence in the process of isotropization. An important energetic aspect of the SMMs is that most of their energy is supplied by the mesoscale eddies by a downscale, or direct transfer. In Yang et al. (2019), for example, it was shown that the submesoscale energy can be maintained by the destruction of mesoscale eddies encountering rough topography. In this respect, the SMMs are similar to their mesoscale counterparts in the atmosphere (Lindborg 1999; Galperin and Sukoriansky 2020) (the latter reference will be referred to as GS20 henceforth). In Zheng et al. (2020), the SMMs were subdivided into 4 different categories whose physics included such diverse processes as internal waves and tides, instabilities and shear waves, spiral trains and trains of coherent vortices, topographic waves, estuary plumes, fronts, vertical mixing, turbulence, and offshore jets and filaments.

Seasonal variability of SMMs has been recognized for its important role in the ocean dynamics as well as global circulation, transport and climate processes (Shcherbina et al. 2015; Callies et al. 2015; Rocha et al. 2016; Su

Responsible Editor: Zhiyu Liu

This article is part of the Topical Collection on the *11th International Workshop on Modeling the Ocean (IWMO), Wuxi, China, 17-20 June 2019*

✉ Boris Galperin
bgalperin@usf.edu

[1] College of Marine Science, University of South Florida, 140 7th Avenue South, St. Petersburg, FL, 33701, USA

[2] Department of Mechanical Engineering, Perlstone Center for Aeronautical Engineering Studies, Ben-Gurion University of the Negev, Beer-Sheva, Israel

[3] Department of Oceanography, University of Hawaii at Manoa, 1000 Pope Road, Honolulu, HI, 96822, USA

et al. 2018; Qiu et al. 2018; Buckingham et al. 2019). The intensity of the SMMs is stronger in winter and weaker in summer. The winter intensification is stipulated by flow straining and development of the deep mixed layer by seasonal winds that modulate mixed layer instabilities (MLIs) and frontogenesis, e.g., Callies et al. (2015), Li et al. (2019), and Zhang et al. (2020).

As an outcome of this variability, one would expect turbulence intensity on the submesoscales to increase in winter and decrease in summer. If the kinetic energy (KE) spectrum on these scales were Kolmogorov-like, then the turbulence intensity could be quantified by the rate of the energy transfer, Π_ε, that enters the expression for the spectrum. The slope of the KE spectrum on submesoscales obtained from numerous observations indeed appears close to Kolmogorov's $-5/3$ but it has also been taken equal to -2, e.g., Sasaki et al. (2014), as would be dictated, for instance, by the Garrett and Munk spectrum for internal gravity waves (Garrett and Munk 1979).

Studies of spectral amplitudes, in addition to the slopes, could have helped to clarify the prevailing physical mechanisms governing the SMMs. However, the slopes have received far more attention in the literature than the amplitudes, even though the latter harbor deeper information on the physics governing dynamical processes. For instance, in the case of the Kolmogorov turbulence, the dimensional analysis enables one to infer the slopes from the dimensions of the variables characterizing the amplitudes, but one can neither deduce these variables uniquely nor determine the amplitudes from the slopes alone.

Difficulties with using Kolmogorov's theory on oceanic submesoscales stem from the fact that it applies to locally homogeneous and isotropic turbulence while the oceanic turbulence is patently anisotropic, e.g., Garrett (2006). In the original Kolmogorov theory, the magnitudes of the slopes of longitudinal and transverse KE spectra are established from the dimensions of the variables forming the spectral amplitudes by virtue of the dimensional analysis. In the case of locally isotropic homogeneous turbulence, the number of variables characterizing the inertial subrange is limited to only two, Π_ε, and the wave number, k. But in anisotropic turbulence, spectral anisotropization and inherent proliferation of the critical dimensional variables hinder the applicability of the dimensional analysis. Progress in that case can only be achieved with an analytical theory that systematically accounts for a contribution of every term in the governing equations. Theories of anisotropic turbulence are scanty, complicated, e.g., Sagaut and Cambon (2018), and difficult to use. As a result, investigations of the SMMs in the framework of anisotropic turbulence are scanty as well. In this paper, however, the emphasis will be put precisely upon anisotropic turbulence using the recently developed analytical theory known as the quasi-normal scale elimination, or QNSE (Sukoriansky et al. 2005; Sukoriansky and Galperin 2016; Galperin and Sukoriansky 2020).

Physical laws governing the spectra of oceanic turbulence apply to atmospheric flows as well. Although a conjecture about the similarity of these flows' spectra has been advanced by Charney (1971) some 50 years ago, its implications have not been fully appreciated. A new impetus towards its exploration emanates from GS20 where it was substantiated in the framework of the QNSE theory. The theoretical underpinning of QNSE is briefly explained in the next section. The horizontal spectra predicted by QNSE as media-independent universal expressions agree well with those derived from numerous atmospheric and oceanic observations. In this paper, the theory is applied to quantify seasonal variability of oceanic flows on submeso- and mesoscales.

Among the existing theories of atmospheric and oceanic turbulence are the ones featuring the unbalanced, strongly nonlinear dynamics, e.g., Lindborg (2006), Lindborg (2015), Vallgren et al. (2011), and Deusebio et al. (2013) and others, connecting to weakly nonlinear inertia-gravity waves (Dewan 1979; VanZandt 1982; Callies et al. 2016) and the Garrett and Munk spectrum (Garrett and Munk 1979).

It was argued in Lindborg and Cho (2001) that the observed highly anisotropic atmospheric flows cannot be explained within the classical three-dimensional (3D) isotropic turbulence. In Lindborg (2006) it was hypothesized that the atmospheric spectra could possibly be attributed to stratified anisotropic turbulence. However, numerical simulations detailed in Skamarock et al. (2014) did not support this hypothesis. A surface quasigeostrophic (SQG) model (Blumen 1978; Juckes 1994; Held et al. 1995; Lapeyre 2017) based upon a premise that a discontinuous profile of the background stratification may lead to a downscale buoyancy variance cascade and a $-5/3$ KE spectrum was used to explain the occurrence of this spectrum on the tropopause mesoscales, i.e., scales up to about 600 km. This model was extended in Tulloch and Smith (2006) and Tulloch and Smith (2009) to also include the -3 spectrum on larger scales. However, as argued in Lindborg (2009), the SQG models are unlikely capable of dealing with the mesoscale atmospheric dynamics because the Rossby numbers at those scales are too large and in addition, the thickness of the layer where the SQG models apply is too shallow. In reply to these arguments in Smith and Tulloch (2009) suggestions were made towards the improvement of the SQG model.

In a study presented in Lovejoy et al. (2009) a spotlight was put on turbulence anisotropy with admonition that a failure to account for different scaling laws in the horizontal

and vertical directions may lead to spurious results. The authors questioned the attribution of the two horizontal scaling regimes to a transition from small-scale 3D isotropic turbulence to a large-scale, two-dimensional (2D), isotropic turbulence and suggested that in anisotropic turbulence, structures progressively flatten out with increasing scale and may obey a power law that is not based upon the dimensional transition. They expressed some scepticism about the fact that "the entire mainstream view of the atmosphere has fundamentally been coloured by the assumption of isotropic turbulence." These and other issues were elaborated in the following up discussions in Lindborg et al. (2009) and Lovejoy (2009).

Most of the existing theories of the spectra on large scales utilize Charney's paradigm of geostrophic turbulence (Charney 1971) according to which a fast rotating, stably stratified 3D flow acquires dynamical properties analogous to those of purely 2D turbulence. Then, the enstrophy conservation gives rise to the enstrophy subrange (Batchelor 1969; Kraichnan 1967; Leith 1968) with the spectrum $\propto \Pi_\omega^{2/3} k_h^{-3}$ on scales smaller than the forcing scale (here, Π_ω denotes the constant spectral enstrophy flux and k_h is the horizontal 2D wavenumber). In Lindborg and Cho (2001) it was stated that there is no alternative to Charney's (Charney 1971) theory that could explain the shape of the second-order structure functions and underlying kinetic energy spectra on atmospheric synoptic scales. The importance of Charney's theory has been reasserted recently in Bierdel et al. (2016): "...there is a wide consensus about the crucial role of quasi-two-dimensional balanced motions in generating the shape of the kinetic energy spectrum on synoptic scales (Charney 1971)..." and in Asselin et al. (2018): "Synoptic-scale dynamics are typically interpreted in the light of Charney's theory of geostrophic turbulence, which predicts a forward enstrophy cascade along a -3 spectrum below the baroclinic injection scale".

One aspect common to all these theories is highlighting the spectral slopes while according little to no attention to the amplitudes. The slopes and the amplitudes are two sides of the same coin, however. Comprehension of the physical processes governing spectral laws requires clear quantitative understanding of both characteristics.

The uncertain situation with theoretical description of atmospheric and oceanic turbulence was recapped in a remark by Yano (2010): "In summary, in spite of appealing nature of the anisotropic turbulence theory that potentially unifies the atmospheric flows of all scales, as it stands for now, it remains a purely statistical theory without a counterpart dynamical model for describing the system in deterministic manner. Such a system should have a capacity of continuously transforming from a quasi-geostrophy to nonhydrostatic anelasticity. My naïve feeling is that an elaborated use of a renormalization group (RNG) theory might potentially lead to a necessary theoretical breakthrough, but I should not be too speculative."

This remark was not too speculative as substantial progress has been achieved with the application of the RNG-based (Yakhot and Orszag 1986) QNSE theory to neutrally stratified, rotating turbulent flows (Sukoriansky and Galperin 2016). QNSE offers a new look at the physics of the effect of rotation and produces analytical expressions for one-dimensional (1D) and 3D spectra that are Coriolis parameter- and, thus, latitude-dependent on large scales. In GS20, these expressions were shown to agree fairly well with numerous atmospheric and oceanic spectra throughout the globe in both the amplitude and the slope.

QNSE does not employ the assumptions of geostrophic turbulence or SQG. Instead, the expressions for the longitudinal and transverse spectra are interpreted in GS20 as an evidence of the compression of the vertical dimension of a flow by rotation in such a way that the total dimensionality appears to become smaller than 3 but larger than 2. In other words, rotating flows can be classified as those with "compactified" (compressed) dimensionality (Celani et al. 2010; Ecke 2017). Flows of this kind may feature both upscale (inverse) and downscale (direct), i.e., *dual* energy cascade (Deusebio et al. 2014; Qiu et al. 2014; Pouquet et al. 2017; King et al. 2015) in the same inertial subrange. There may exist a transition, either continuous or discontinuous, between the scales with opposite cascade directions, e.g., Sahoo et al. (2017). An example of such transition was detected in the hurricane vortices where the cascade changed sign with altitude (Byrne and Zhang 2013).

In GS20 it was concluded that in oceanic flows on mesoscales, the spectral amplitudes are determined by the Coriolis parameter rather than the spectral energy/enstrophy fluxes. For the first time, the latitudinal dependence of the spectral amplitudes was detailed within a rigorous theory. Another important outcome was the possibility of estimating the rate of the energy transfer, Π_ε, from meso- to submesoscales. This rate can exceed the microstructure dissipation rate by one or more orders of magnitude. Since, on the one hand, Π_ε represents the spectral energy flux in the Kolmogorov spectra and on the other, it characterizes collective dissipation processes throughout the submesoscales, it was termed in GS20 *effective submesoscale dissipation*, or ESD.

This paper will focus upon the seasonal variability of the ESD. Its values will be estimated from the spectra available from observations in the North-West Atlantic (Shcherbina et al. 2015; Callies et al. 2015) and North-West Pacific Oceans (Qiu et al. 2017).

The paper is structured in the following manner. Section 2 provides a brief survey of the QNSE theory of

rotating flows. Section 3 elaborates the application of the QNSE results to oceanic turbulence. Section 4 provides characterization of the turbulence's seasonal variability in terms of ESD, and Section 5 is discussion and conclusions.

2 A brief survey of the QNSE results for rotating turbulence

The QNSE theory of rotating turbulence was developed in Sukoriansky and Galperin (2016). The theory considers neutrally stratified, 3D, incompressible (i.e., solenoidal) rotating flows in an unbounded domain. QNSE accounts for the interaction of turbulence and inertial waves. As the geostrophic approximation is not invoked, the theory does not differentiate between geostrophic and ageostrophic, balanced and unbalanced motions. As argued in GS20, this patently "minimalistic" albeit fully nonlinear framework provides an adequate approximations for the 1D spectra of the horizontal velocities throughout the oceanic meso- and submesoscales. As an illustration of the successes of the theory, one can recall the reproduction of the Nastrom and Gage spectra (Nastrom et al. 1984) in the upper troposphere and lower stratosphere.

Let $f = 2\Omega \sin\theta$ be the Coriolis parameter with Ω and θ being the angular velocity of the Earth's rotation and the latitude, respectively. Denote the components of a horizontal wave vector $\mathbf{k}$ by k_1 and k_2, respectively. The QNSE expressions for the longitudinal ($E_1(k_1)$) and transverse ($E_2(k_1)$) spectra of the horizontal velocity variance relative to the direction k_1 and in the limit of a weak rotation are (Sukoriansky and Galperin 2016)

$$E_1(k_1) = \frac{18}{55} C_K \Pi_\varepsilon^{2/3} k_1^{-5/3} + C_{f1} f^2 k_1^{-3}, \tag{1}$$

$$E_2(k_1) = \frac{24}{55} C_K \Pi_\varepsilon^{2/3} k_1^{-5/3} + C_{f2} f^2 k_1^{-3}, \tag{2}$$

where $C_K \simeq 1.5$ is the Kolmogorov constant, $C_{f1} = 0.0926$ and $C_{f2} = 0.24$. The vertical direction and vertical spectral component will not be considered here as they depend on stable stratification and are out of the scope of this paper.

Rotation renders 3D turbulence anisotropic yet it preserves the horizontal quasi-isotropy in the f-plane approximation: although the two longitudinal ($E_1(k_1) \equiv E_L(k_1)$ and $E_2(k_2) \equiv E_L(k_2)$) and two transverse ($E_2(k_1) \equiv E_T(k_1)$ and $E_1(k_2) \equiv E_T(k_2)$) spectra are congruent, the isotropic relationship between $E_1(k_1)$, $E_2(k_1)$ and the total spectrum, $E(k)$, derived in Monin and Yaglom (1975) holds only for the Kolmogorov branch and is violated in its Coriolis counterpart. This can be shown by direct substitution of (1) and (2) in the analytical expression relating $E_1(k_1)$ and $E_2(k_1)$ in isotropic solenoidal 3D flows derived in Monin and Yaglom (1975),

$$E_2(k_1) = \frac{1}{2}\left[E_1(k_1) - k_1 \frac{\mathrm{d}E_1(k_1)}{\mathrm{d}k_1}\right]. \tag{3}$$

More details can be found in GS20.

In GS20 it was argued that (1) and (2) are expected to provide good approximation to spectra in natural flows when rotational effects dominate on the horizontal scales while stable stratification dominates on the vertical scales, i.e., $f/N \ll 1$, where N is the Brunt-Väisälä frequency. This argument was backed by demonstrating good agreement between (1) and (2) and atmospheric and oceanic spectra at many different locations.

Equations (1) and (2) can be viewed as a generalization of the classical Kolmogorov spectra to rotating flows. The spectra exhibit superposition of the Kolmogorov and f-dependent (Coriolis) branches with the wave-turbulence crossover scale proportional to the Woods scale, $L_\Omega = (\Pi_\varepsilon/f^3)^{1/2}$, which is a rotational analogue of the Ozmidov scale, $L_O = (\Pi_\varepsilon/N^3)^{1/2}$, in turbulent flows with stable stratification. In this formulation, both the Woods and Ozmidov scales are considered in the generalized form whereas the energy flux, Π_ε, replaces the dissipation rate, ε. Further discussion of the analogy between L_O and L_Ω can be found in Sukoriansky and Galperin (2016).

The crossover scale between the Kolmogorov and Coriolis branches can be defined by equating the two terms in (1). In terms of the length scale, this crossover is

$$L_c \simeq 5.4^{3/4} L_\Omega \simeq 3.5 L_\Omega. \tag{4}$$

In GS20 it was shown that the development of the Kolmogorov spectrum is a rather common phenomenon on oceanic submesoscales that gives rise to the ESD. Thus, the scale L_c could be associated with the upper bound of SMMs. A taxonomy of these motions is given in Zheng et al. (2020).

If the energetics of the SMMs variability can indeed be encapsulated in one parameter, Π_ε, then the scale L_c, along with Π_ε, can be viewed as a measure of that variability. If the Kolmogorov branch of the spectrum roughly coincides with the extent of the submesoscale, then L_c can be viewed as a characteristic scale of the SMMs and its seasonal variation mirrors that of the submesoscale turbulence.

Another measure of the SMMs variability was introduced in Qiu et al. (2018) and denoted L_t. That length scale defines a crossover between the balanced and unbalanced motions. While L_c pertains strictly to the threshold of the Kolmogorov spectrum, the scale L_t characterizes relative importance of the wave processes. Considered on seasonal time scales, these length scales characterize different aspects of the variability.

Equations (1) and (2) provide an important quantitative characterization of the submeso- and mesoscale variabilities. The former is driven by submesoscale processes that may change Π_ε in a wide range and cause large variations of the spectral amplitude. The latter, being determined by the Coriolis parameter, is rather limited and can be predicted. One can expect that observed and simulated spectra would converge to a single line on the low wave number end of the mesoscales. The size of the eddies can influence the mesoscale KE variability via modification of the low wave number end of the spectrum that contains high energy. The variability of these eddies is not universal and can be best assessed with satellite altimetry.

3 Seasonal variability of oceanic turbulence: an analytical framework

A high-resolution simulation of a large area in the North Pacific ocean undertaken in Sasaki et al. (2014) focused on oceanic variability caused by MLI induced by synoptic wind fluctuations. In addition to the atmospheric forcing, a strong mesoscale strain field can also be a source of MLI (Zhang et al. 2020). Judging by the results in Sasaki et al. (2014) one infers that the MLI has a significant effect on the oceanic submesoscales while the variability on mesoscales is limited. Indeed, as evident in Fig. 5a in Sasaki et al. (2014), large differences in the circulation features between March and September shown in Fig. 1 of that paper had almost no effect on spectral amplitudes on the mesoscales. This important result is consistent with the QNSE theory that predicts the dependence of spectral amplitudes in the mesoscales range on the Coriolis parameter only.

To ascertain the quantitative conformity between the theory and simulations in Sasaki et al. (2014), we use a QNSE-based expression for the horizontal KE spectrum, $E_h(k_h)$, k_h being the horizontal wave number, as derived from the general theory in Sukoriansky and Galperin (2016),

$$E_h(k_h) = \frac{7}{110} B\left(\frac{1}{6}, \frac{1}{3}\right) C_K \Pi_\varepsilon^{2/3} k_h^{-5/3} + C_f f^2 k_h^{-3}. \quad (5)$$

Here, $B(p, q)$ is a Beta-function, $(7/110)B(1/6, 1/3) \simeq 0.535$, $C_f = 0.33$. Only the Kolmogorov (i.e., the submesoscale) branch in (5) depends on Π_ε. The theoretical spectral amplitude on mesoscales is solely determined by the Coriolis parameter.

The expression for the first term in (5) is not well known and so it is derived here using the classical expression relating the spectrum tensor, $F_{ij}(\boldsymbol{k})$, to the 3D energy spectrum, $E(k)$, where $\mathbf{k}$ is the 3D wave vector and k is its magnitude (Monin and Yaglom 1975),

$$F_{ij}(\boldsymbol{k}) = \frac{E(k)}{4\pi k^2} P_{ij}(\boldsymbol{k}). \quad (6)$$

Here, $P_{ij}(\boldsymbol{k}) = \delta_{ij} - k_i k_j / k^2$ is the projection operator and δ_{ij} is the Kronecker δ-symbol. For the 3D Kolmogorov spectrum, $E(k)$ is

$$E(k) = C_K \Pi_\varepsilon^{2/3} k^{-5/3}. \quad (7)$$

After separating $\boldsymbol{k}$ into its horizontal, k_h, and vertical, k_z, components, the horizontal part of $F_{ij}(\boldsymbol{k})$ takes the form

$$F_h(k_h, k_z) = \frac{C_K \Pi_\varepsilon^{2/3}}{4\pi (k_z^2 + k_h^2)^{11/6}} \left(2 - \frac{k_h^2}{k_z^2 + k_h^2}\right). \quad (8)$$

The integration of (8) in the vertical yields an expression for the spectrum of the horizontal KE as a function of k_h,

$$\begin{aligned} E_h(k_h) &= \pi k_h \int_{-\infty}^{\infty} F_h(k_h, k_z) dk_z \\ &= \frac{7}{110} \frac{\Gamma\left(\frac{1}{6}\right) \Gamma\left(\frac{1}{3}\right)}{\pi^{1/2}} C_K \Pi_\varepsilon^{2/3} k_h^{-5/3} \\ &= \frac{7}{110} B\left(\frac{1}{3}, \frac{1}{6}\right) C_K \Pi_\varepsilon^{2/3} k_h^{-5/3}. \end{aligned} \quad (9)$$

In (9), $\Gamma(x)$ is the gamma function. Equation (9) is in a good agreement with the simulations of stably stratified turbulence presented in Kimura and Herring (2012). These simulations show a weak dependence of the horizontal spectra on stable stratification. The spectra preserved their Kolmogorov shape, including the coefficients, even for strong stable stratification thus providing an a posteriori justification for the application of the QNSE theory to stably stratified flows such as the oceanic ones. The derivation of the horizontally anisotropic Coriolis branch, which is the second term on the right-hand side of (5), is considerably more complicated and cannot be detailed here.

To ascertain the validity of the QNSE-based predictions, (5) was compared with the results of a realistic high-resolution numerical simulation of the North Pacific Ocean presented in Sasaki et al. (2014), their Fig. 5a. The latitude in (5) was set at $\theta = 30°$ which corresponds to the middle of the computational domain confined between 20° N and 43° N. The comparison, shown in Fig. 1, reveals different tendencies on submeso- and mesoscales. Let us consider the former first.

One notices a rapid decrease of the simulated spectra on submesoscales. Quantitative accommodation of this decrease within the QNSE theory requires Π_ε to be of the order of 10^{-9} m^2 s^{-3}. The KE fluxes calculated from geostrophic velocities and shown on Fig. 5d in Sasaki et al. (2014) are of a similar order of magnitude. However, these values are some 3 orders of magnitude smaller than an average ESD (=Π_ε), of the order of 10^{-6} m^2 s^{-3}, as evaluated in GS20 based upon the data collected by ship-mounted acoustic Doppler current profilers (ADCPs) throughout the world ocean. There exists a possibility that in

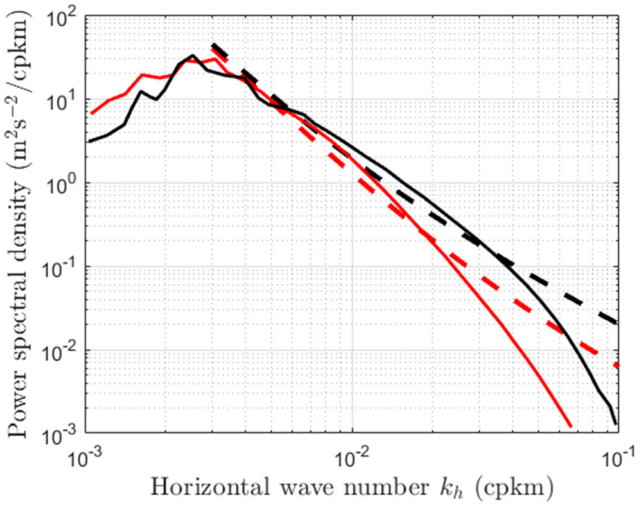

Fig. 1 Spectra of the horizontal velocity in the North Pacific, as computed in simulations in Sasaki et al. (2014), their Fig. 5a, and shown as black and red solid lines for March 2002 and September 2002, respectively. The QNSE expression (5) for $\theta = 30°$ N is shown by the black and red dashed lines for $\Pi_\varepsilon = 7 \times 10^{-6}$ m^2 s^{-3} and 10^{-6} m^2 s^{-3}, respectively. Compared with the theoretical expressions, the modeled spectra appear to be over-damped on submesoscales

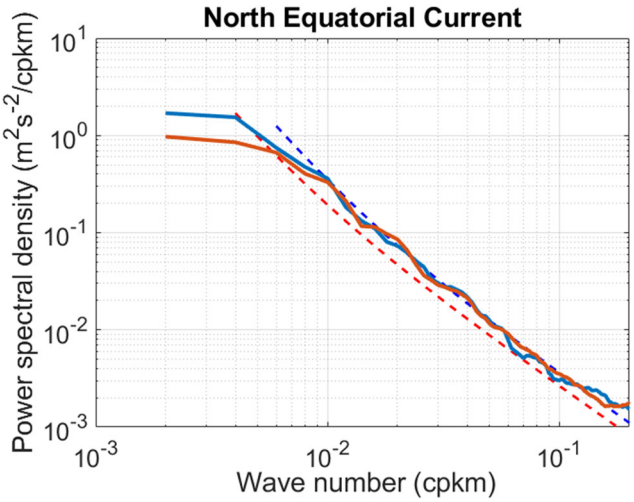

Fig. 2 Longitudinal (red) and transverse (blue) spectra obtained along 137°E meridian in the North-Western Pacific in the vicinity of the North Equatorial Current (NEC), at the latitude $\theta = 14°$ N. The data is from Qiu et al. (2017) where the spectra were averaged over the depths between 40 and 100 m. The dashed red and blue lines are (1) and (2), respectively, with the estimated value of Π_ε of 2×10^{-6} m^2 s^{-3}. The figure is adapted after Galperin and Sukoriansky (2020)

the model, the fluxes are over-damped by a chosen subgrid-scale (SGS) parameterization scheme and/or numerical viscosity (Schubert et al. 2020). A similar over-damping is notable in other studies. Among those is the comparison of the QNSE predictions with high-resolution simulations (1/48°) of the horizontal spectra near Drake Passage with MITgcm (Rocha et al. 2016) shown on the lower panel of Fig. 9 in GS20. Another example is a simulation of the Agulhas Current system in Schubert et al. (2020), their Fig. 2a. As evident in Fig. 1 here, the over-damping affects the entire submesoscale range because not only the value of Π_ε is too small but also the shape of the theoretical spectrum is not congruent to the shape of its numerical counterpart.

One can question, however, whether or not the behavior of the theoretical spectrum on submesoscales is realistic and whether or not it provides a good quantitative approximation to the data. To ascertain the accuracy of theoretical predictions, Fig. 2 compares the QNSE-based 1D spectra along the longitude 137° E in the region of the North Equatorial Current, or NEC, with the multi-year averaged spectra estimated with a ship-mounted ADCP reported in Qiu et al. (2017). The figure demonstrates a good agreement between the theoretical and observational spectra in the entire wave number range that includes both submeso- and mesoscales. In GS20, an equally good agreement between the theory and data is shown in many other locations throughout the world ocean.

On mesoscales, an agreement between the theory and numerical simulations improves. A good correspondence between the QNSE-based and computational spectra on scales exceeding about 50 km is achieved with realistic values of Π_ε, 7×10^{-6} m^2 s^{-3} and 1×10^{-6}m^2 s^{-3} for March and September, respectively. All spectra converge to a single line well described by (5) which is an indication that the spectral amplitudes in this subrange are prevalently determined by the Coriolis parameter.

The latter is an important result on its own sake. Recall that according to Fig. 5d in Sasaki et al. (2014), the mesoscales feature an inverse energy cascade with a non-constant, scale-dependent energy flux while the spectral amplitudes are determined by the Coriolis parameter rather than the energy or enstrophy fluxes. This outcome confirms the QNSE theory prediction.

In a more general context, the oceanic meso- and submesoscales harbor the coexisting direct and inverse energy cascades, termed the *dual* cascade, e.g., Deusebio et al. (2014), Qiu et al. (2014), Pouquet et al. (2017), King et al. (2015), and Wang et al. (2015), that often develops in flows with extra strains, i.e., strains additional to the basic shear. Flows of this kind were first considered in detail in Bradshaw (1973). As explained in GS20, in a certain subrange of governing parameters, spectral amplitudes in such flows are determined by the magnitude of the extra strains (f^2 in the case of rotating flows) rather than the energy/enstrophy fluxes.

Of importance, the spectral KE fluxes on submesoscales are positive, both in the theory, as explained in Sukoriansky and Galperin (2016), and in simulations, as evident in Fig. 5a in Sasaki et al. (2014), pointing to a direct energy cascade. A direct cascade on submesoscales was also

detected in observational studies such as, for instance, those employing drifters as described in Poje et al. (2017) and others, e.g., D'Asaro et al. (2011), Zhang et al. (2016), and Gula et al. (2016). One needs to keep in mind that the effect of rotation leads to redirection of a part of the direct cascade upscales and that the partition of the cascade is scale-dependent. Nevertheless, the Kolmogorov's $-5/3$ spectral law appears to remain a good approximation over the entire submesoscale range and provide a single value of Π_ε that represents the average downscale energy flux. Precisely this property of Π_ε is behind the introduction of the notion of ESD in GS20. In a general context, the applicability of the Kolmogorov spectral laws beyond strictly specified inertial subranges has been well known and inspired various explanations such as that in Golitsyn (2018). In oceanic mixed layers characterized by very strong anisotropy (horizontal and vertical scales of about 10 km and 1 km, respectively), the validity of the Kolmogorov spectrum in the horizontal can be explained by a superposition of the effects of rotation and stable stratification. Indeed, as was shown in Galperin and Sukoriansky (2010) and Sukoriansky and Galperin (2013), in stratified flows, the Kolmogorov spectrum prevails on scales exceeding the layering scales. A more detailed discussion of these issues is beyond the scope of the present paper.

Concluding this section, we reiterate that the comparison with simulations supports the initial QNSE theory-based hypothesis that the variability of the submesoscale turbulence can be quantified in terms of a single parameter, ESD ($=\Pi_\varepsilon$), even though the turbulence may have many sources. It can be produced by diverse factors such as breaking waves, instabilities, and tidal flows. Different aspects of the commingling between waves and turbulence have been addressed in the literature over the years as, for instance, in Dritschel and McIntyre (2008), McIntyre (2008), Wood and McIntyre (2010), and Galperin et al. (2014), where it was clarified that in high-Reynolds-number geophysical flows, there are no waves without turbulence and there is no turbulence without waves. In other words, waves and turbulence always coexist. In terms of the scale L_c given by (4), it was around 6 km in summer and 15 km in winter for the QNSE emulation of simulations in Sasaki et al. (2014) shown in Fig. 1. This scale quantifies the horizontal extent of the Kolmogorov turbulence subrange and can be viewed as an additional characteristic of the submesoscale turbulence and its seasonal variability.

4 Seasonal variability of oceanic turbulence—comparisons with data

Further analysis of the seasonal oceanic variability on meso- and submesoscales will be given via comparison of the theoretical predictions with data collected by ship-mounted ADCPs in the course of three different observational programs. Two of these programs, Oleander and LatMix, were carried out in the vicinity of the Gulf Stream. The third program was conducted in the North-West Pacific Ocean along the meridian 137° E as described in Qiu et al. (2017). Comparisons between the theory and observations are presented in the next three subsections.

4.1 Oleander observations

Both data collection programs, Oleander and LatMix, are described in Callies et al. (2015). Locations of the data transects are shown in Fig. 3. The data from these programs was described in Shcherbina et al. (2013) and processed in Callies et al. (2015) where a full description of the data can be found. The spectral results were digitized using a freely available software package (https://apps.automeris.io/wpd/) and used to produce Figs. 4 and 5 in this paper.

Long-term velocity and temperature data have been collected by the CMV *Oleander* during its weekly cruises between New York Harbor and Bermuda. The data from the time window between 2005 and 2013 was used to study the seasonal variation of the velocity and temperature spectra in the vicinity of the Gulf Stream (Callies et al. 2015). In the paper, half the sum, $(1/2)[E_L(k_1) + E_T(k_1)]$, was defined as the 1D spectrum of the horizontal turbulence KE. A more conventional definition of such spectrum would involve the horizontal wave number k_h leading to (9). However, to be consistent with the data in Callies et al. (2015), we shall use their definition in the forthcoming comparisons.

Figure 4a compares the defined above 1D spectra at the depth of 50 m collected during winters and summers with the QNSE predictions. The average location of the transects was set at 31° N. One notices a good agreement between the theory and the data for spectral amplitudes and slopes in the entire range of the wave numbers for both seasons. On mesoscales, consistent with the results in Sasaki et al. (2014) discussed in the previous section, the seasonal variability is weak and the spectral amplitudes converge to the value given in (5) as determined by the Coriolis parameter. On submesoscales, however, the variability is clearly attributable to changes in turbulence intensity. It can be quantified in terms of the energy flux Π_ε, or ESD that varies by about an order of magnitude, from 1.5×10^{-5} $m^2\ s^{-3}$ in winter to 2×10^{-6} $m^2\ s^{-3}$ in summer. The scale L_c fluctuates from about 21 km in winter to about 8 km in summer. Thus, Π_ε and L_c provide important characteristics of the intensity and the length scale of the submesoscale turbulence and its seasonal variation.

Figure 4b compares theoretical and data-based longitudinal and transverse spectra averaged over the winter season.

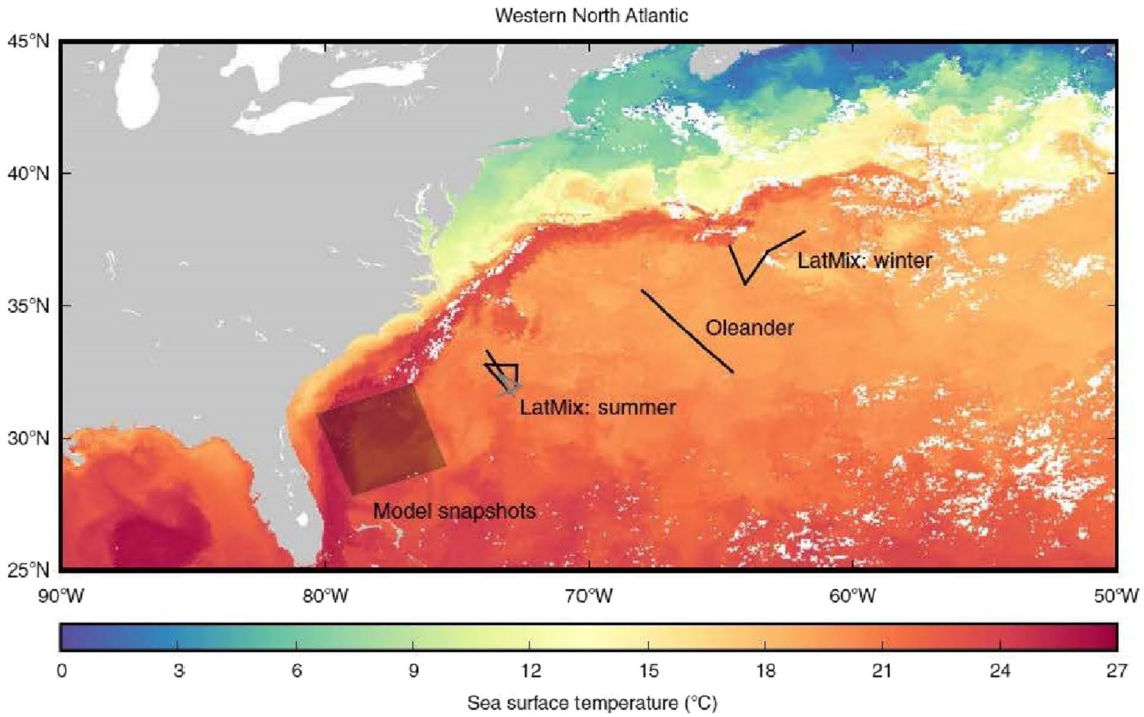

Fig. 3 Measurement locations for the Oleander and LatMix programs. Black lines show velocity transects. The color shading describes the variation of the sea surface temperatures on 13–20 March 2012. White shading points to missing data. Adapted from Callies et al. (2015)

The theory reliably approximates observationally determined spectral slopes and amplitudes on both meso- and submesoscales. The transverse spectrum exceeds its longitudinal counterpart thereby pointing to flow solenoidality.

4.2 LatMix observations

Another investigation of the seasonal variability of the near-surface ocean dynamics in the vicinity of the Gulf Stream was conducted in the framework of the Lateral Mixing Experiment (LatMix) along several transects off Cape Hatteras in June 2011 (designated as summer) and just south of the Gulf Stream extension in March 2012 (designated as winter) (Shcherbina et al. 2013; Callies et al. 2015). Figure 5a compares the 1D quantity $(1/2)[E_L(k_1) + E_T(k_1)]$ as estimated from the data and the theory in the format analogous to Fig. 4a. Even though the data and the theory exhibit similar trends and the spectra tend to

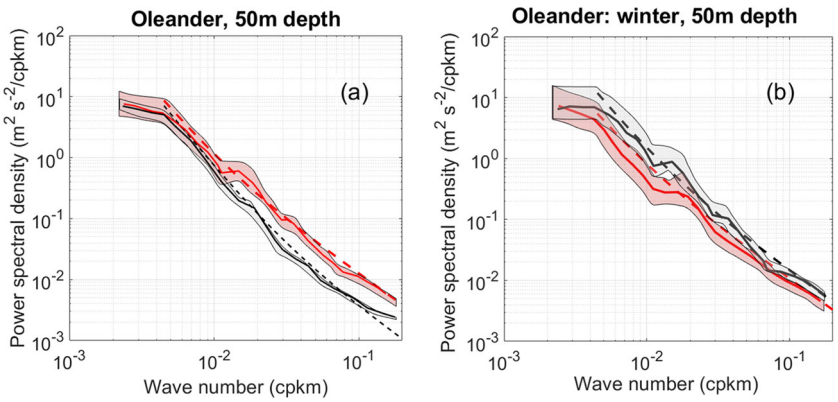

Fig. 4 (a) Seasonal variation of the quantity $(1/2)[E_L(k_1) + E_T(k_1)]$ deduced from the Oleander data for winter and summer, red and black solid lines, respectively, at the depth of 50 m, as compared with the QNSE predictions shown in dashed lines. The QNSE results are obtained for $\theta = 31°$ N, $\Pi_\varepsilon = 1.5 \times 10^{-5}$ m^2 s^{-3} and $L_c \simeq 21$ km in winter and $\Pi_\varepsilon = 2 \times 10^{-6}$ m^2 s^{-3} and $L_c \simeq 8$ km in summer. (b) Longitudinal (solid red) and transverse (solid black) KE spectra for the Oleander data vs. QNSE theory (dashed red and dashed black, respectively) for winter. The parameters employed in QNSE are $\theta = 31°$ N, $\Pi_\varepsilon = 1.5 \times 10^{-5}$m^2 s^{-3}, and $L_c \simeq 21$ km. The light shadings on both panels show the 95% confidence intervals. The data is adapted from Callies et al. (2015)

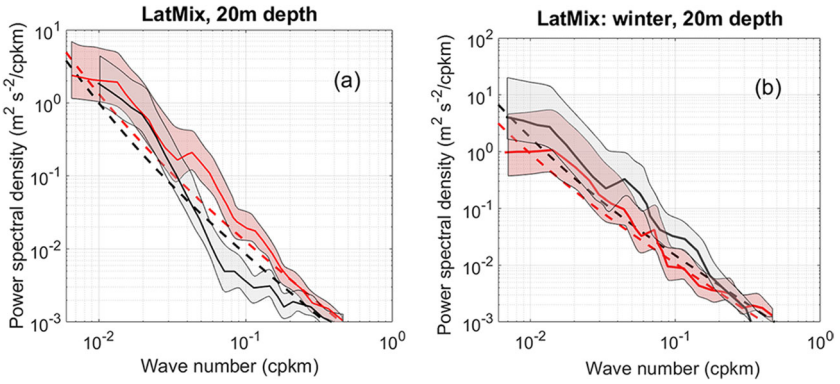

Fig. 5 (a) Seasonal variation of the quantity $(1/2)[E_L(k_1) + E_T(k_1)]$ deduced from the LatMix data for winter and summer at the depth of 20 m, red and black solid lines, respectively, as compared with the QNSE predictions shown in dashed lines. The QNSE results are obtained with $\theta = 36°$ N, $\Pi_\varepsilon = 1.5 \times 10^{-5}$m^2 s^{-3}, and $L_c \simeq 17$ km in winter and $\theta = 32°$ N, $\Pi_\varepsilon = 8 \times 10^{-6}$m^2 s^{-3}, and $L_c \simeq 15$ km in summer. (b) Longitudinal (solid red) and transverse (solid black) KE spectra for the LatMix data at the depth of 20 m vs. QNSE theory (dashed red and dashed black, respectively) for winter. The parameters employed in QNSE are $\theta = 36°$ N, $\Pi_\varepsilon = 1.5 \times 10^{-5}$m^2 s^{-3}, and $L_c \simeq 17$ km. The light shadings on both panels show the 95% confidence intervals. The data panel is adapted from Callies et al. (2015)

converge closer on mesoscales, the differences are marked. There are two main reasons for these differences. First, the length of the observational record was very short, only one month for winter and summer each. Such records are insufficient for reliable determination of the mean spectra and as a result, the 95% confidence limits in Fig. 5 are much broader than those in Fig. 4. Second, the sites of the LatMix experiment were quite close to the Gulf Stream and the results could be affected by the mean current and the induced by it anisotropy. A study in Wang et al. (2010) demonstrates that the Gulf Stream renders turbulence strongly anisotropic while our own investigation detailed in GS20 showed that in addition, spectral amplitudes on large scales become significantly enhanced. The latter study also revealed that when the study area is distanced from the Gulf Stream, the agreement between the observed and theoretical spectra improves. In a study in Bühler et al. (2017), a special procedure was designed to alleviate the effect of the mean flow anisotropy. That paper did not consider the seasonal variability of the flows, however.

The tendency to increased spectral amplitudes in the vicinity of the Gulf Stream manifests even clearer in Fig. 5b that shows the longitudinal and transverse KE spectra obtained in the LatMix observations. On mesoscales, the amplitudes of both longitudinal and transverse spectra are higher than those predicted by the QNSE theory. On submesoscales, however, despite the shortness of the record, the theory provides reasonable approximation to the data such that the value of Π_ε can be estimated with sufficient precision for use in SGS parameterizations in numerical simulations.

4.3 North-Western Pacific observations

For this study, we used the shipboard ADCP data presented in Qiu et al. (2017). The data was collected by the Japan Meteorological Agency (JMA) along the 137° E meridian, between 3° N and 34° N. The study area is shown in Fig. 6 along with the map of the eddy KE derived from the multi-year AVISO (Archiving Validation and Interpretation of Satellite Data in Oceanography; www.aviso.oceanobs.com). All observational spectra are averaged over the depths between 40 and 100 m.

The area from Japan in the north to 28° N contains the Kuroshio, the western boundary current of the wind-driven subtropical gyre. Like the Gulf Stream after its separation, the intense surface Kuroshio current is accompanied by enhanced mesoscale eddy variability maintained by the mixed baroclinic-barotropic instabilities. The band 14–28° N contains the subtropical countercurrent (STCC). The eastward-flowing STCC overlies the westward-flowing North Equatorial Current (NEC). Although the NEC is a strong westward-flowing wind-driven confluent flow, it is relatively stable compared to the other three current systems of the North-Western Pacific. Nearly constant potential vorticity (PV) gradient across the NEC region is the cause of the relative stability of NEC. The North Equatorial Countercurrent (NECC) lies between 3° and 7° N. Being an eastward-moving outflow of the low-latitude western boundary current, the NECC is highly unstable with horizontal scales in excess of 200 km. It derives its energy mostly from the horizontal shear of the NECC via barotropic instability.

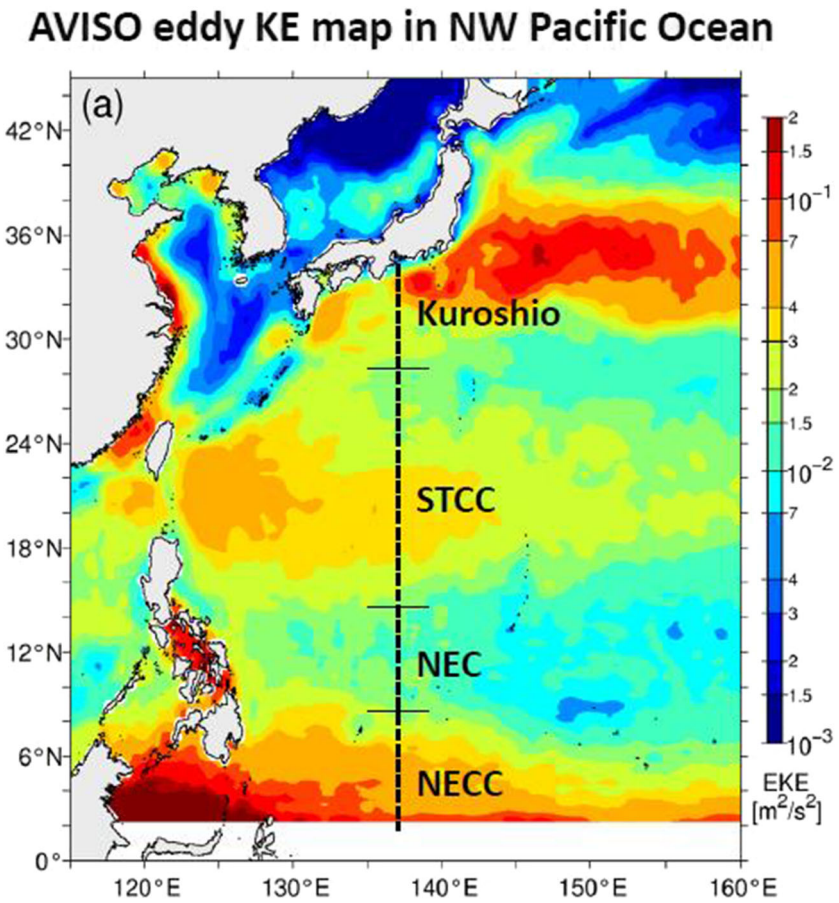

Fig. 6 Regional eddy variability and ADCP track. Surface eddy kinetic energy distribution in the North-Western Pacific based on the weekly AVISO SSH anomaly data of 2004–2015. Black dashed line along 137° E denotes the track of repeated shipboard ADCP measurements by Japan Meteorological Agency. Short black lines along 28° N, 14° N and 9° N demarcate the boundaries of the Kuroshio, STCC, NEC and NECC bands. Adapted from Qiu et al. (2017)

Figures 7 and 8 show seasonal KE spectra in the four regions while Table 1 quantifies these spectra and their variability in terms of Π_ε (or ESD) and L_c.

As shown in Fig. 7, the seasonal variation of the subtropical Kuroshio and STCC bands differ from each other. The former encompasses the western boundary current that, just like the Gulf Stream in the North-Western Atlantic, induces spectral anisotropy. To account for the effect of this anisotropy, a special mathematical procedure was developed in Bühler et al. (2017). As shown in GS20, this procedure reduces spectral amplitudes and renders them closer to QNSE predictions. In a similar fashion, Kuroshio likely introduces spectral anisotropy enhanced by MLI (Qiu et al. 2017) in winter. Since the procedure by Bühler et al. (2017) was not applied, the observed spectral amplitudes in winter are larger than the QNSE prediction, red lines in Fig. 7a. In summer, however, the MLI weakens, the anisotropy likely becomes less pronounced, and the observed amplitude is in a better agreement with QNSE, blue lines in Fig. 7a.

A study in Dong et al. (2020) that used the MITgcm model analyzed the seasonal variability of the energy fluxes

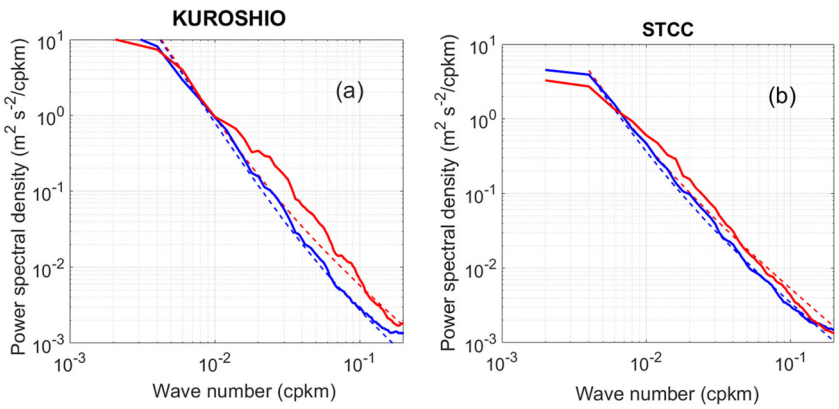

Fig. 7 Seasonal variation of the quantity $(1/2)[E_L(k_1) + E_T(k_1)]$ deduced from the ADCP data in the North-West Pacific Ocean in the Kuroshio (a) and STCC (b) bands for winter and summer, red and blue solid lines, respectively. They are compared with the QNSE predictions shown by respective dashed lines. The data is given in Table 1

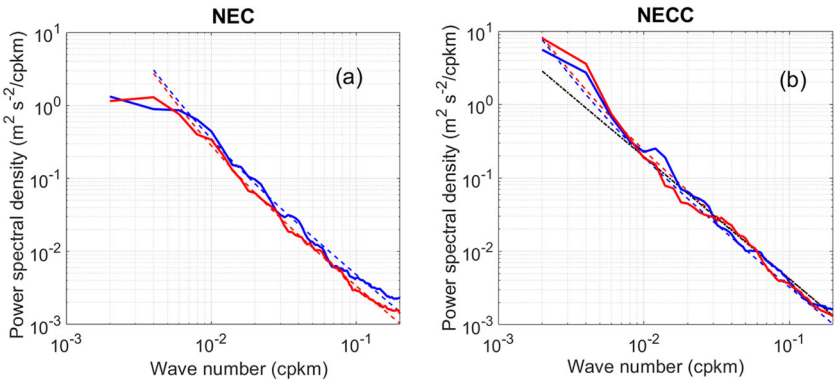

Fig. 8 Same as in Fig. 7 but for NEC (a) and NECC (b). The black dash-dotted line in (b) shows the Kolmogorov branch of the spectrum

across scales as related to the buoyancy production and the mixed layer depth (MLD). This analysis considered not only seasonal but also monthly variability which, in principle, could also be represented in terms of Π_ε and L_c. However, since the QNSE theory in its current form does not include the thermodynamics, such analysis is beyond the scope of this paper.

Similarly to the Kuroshio band, its STCC counterpart also develops deep winter mixed layer prone to MLI on submesoscales (Sasaki et al. 2014; Qiu et al. 2014). Figure 7b indicates that the effect of turbulence anisotropy may persevere in winter causing some discrepancy between the observed and predicted spectra. In summer, however, this effect virtually disappears and the QNSE prediction attains a good agreement with observations.

Quantifying the visual results, Table 1 shows that for both the Kuroshio and STCC bands, the estimated winter values of Π_ε and L_c exceed their summer counterparts while their annual averages are bounded by the seasonal ones. Of importance, towards long mesoscales, spectra converge to QNSE-predicted values determined by the Coriolis parameter.

The tropical region south of 14° N that encompasses NEC and NECC exhibits no appreciable seasonal change of MLD. Accordingly, Fig. 8 shows that the variability of the spectra in these bands is quite anemic. For the NEC band, the seasonal cycle of ESD and L_c is opposite to those for the Kuroshio and STCC bands while for NECC, the cycles are in phase but the summer-winter contrast is quite weak. Dynamically, the summer eddy KE enhancement is related to the adjustment of the surface wind-forced upper ocean across the North Pacific basin. Specifically, the seasonal surface wind forcing over the Pacific Ocean has a winter maximum and is coherent across the wide Pacific Ocean basin. The wind-forced upper oceanic anomalies propagate westward with the speed of the baroclinic Rossby waves of about 0.15–0.30 m s^{-1} (Chelton and Schlax 1996) in the NEC-NECC latitudes. The waves are baroclinically unstable and produce intermittent turbulence with a dual cascade that for the NEC and NECC bands generally peaks in summer. As evident in Fig. 8, this mechanism produces energy spectra with intermittently fluctuating amplitudes. But such behavior appears inconsistent with (5) predicting that on large scales, spectral amplitudes depend on the Coriolis parameter only. This contradiction is resolved by noting a close proximity of the NECC band to the equator where the effect of the Coriolis parameter diminishes. This fact manifests in a large value of L_c, about 60 km. The large extent of the Kolmogorov subrange is also evident in Fig. 8b where the Kolmogorov part of the expression $(1/2)[E_L(k_1) + E_T(k_1)]$ is shown along with full observed spectra. The Kolmogorov expression

Table 1 Annual and seasonal values of Π_ε and L_c in the North-Western Pacific

Region	Latitude, ° N	Annual		Seasonal			
				Winter		Summer	
		Π_ε	L_c	Π_ε	L_c	Π_ε	L_c
Kuroshio	34	3	8.3	4	9.5	1	4.8
STCC	18	3	20	4	23.2	2	16.4
NEC	14	2	24	2	24	3.5	31
NECC	8	3	67	3	67	2	54

$\Pi_\varepsilon \times 10^{-6}$ is in m^2 s^{-3}, L_c is in km; the annual data is from GS20

provides good approximation for the data for scales up to about 200 km, i.e., the entire range exhibiting intermittent fluctuations of spectral amplitudes around Kolmogorov's profile. On larger scales, consistent with (5), winter and summer spectral amplitudes are well represented by the Coriolis part of (5) and nearly merge.

The visual results are quantified in terms of Π_ε and L_c in Table 1. Once again, the seasonal values of these variables bound their corresponding annual values.

It is of interest to compare the scale L_c with the transition length scale L_t introduced in Qiu et al. (2017) and marking the separation between the balanced geostrophic flows and unbalanced internal waves. The results for L_t are summarized in Table 2. Since the QNSE theory in its present form excludes internal waves, this comparison can only be descriptive. Both L_c and L_t tend to grow with decreasing latitude which reflects the decreasing influence of the Coriolis parameter, f, towards the equator. In Qiu et al. (2017), L_t was found to strongly depend on the energy level of local mesoscale eddy variability and so it may exceed 200 km in a relatively stable NEC. In the QNSE theory, on the other hand, L_c is determined by Π_ε and f and as those parameters do not significantly differ from the corresponding neighboring values, so does L_c.

One of the reviewers asked two interesting questions concerning potential failures of the QNSE theory in the equatorial region where the vertical component of the Coriolis parameter, f, vanishes. One question was concerned with the effect of the so-called non-traditional component of the Coriolis parameter, f_y, and the other one regarded a possible importance of the β-effect as in the absence of f, the equatorial dynamics is sensitive to the β-term, β being the latitudinal gradient of f.

With regard to the first question, note that this paper deals with the horizontal KE as a function of the horizontal wave number. On large scales, the horizontal spectra depend on f. The theory was derived for any value of f including zero. The theoretical expressions were tested in GS20 at many different latitudes and longitudes, including the equatorial region, and every test demonstrated a good agreement between the predicted and observed spectra.

To assess the importance of the β-effect in the equatorial region, one can compute its characteristic length scale, $L_\beta = 2\pi(\Pi_\varepsilon/\beta^3)^{1/5}$ (Galperin and Read 2019), which, with $\Pi_\varepsilon = 2 \times 10^{-6}$ m^2 s^{-3} and $\beta = 2.3 \times 10^{-11}$ m^{-1} s^{-1}, yields $L_\beta \simeq$1,100 km. Thus, on scales smaller than about 1,100 km, the β-effect is small and the longitudinal spectrum remains horizontally isotropic and well approximated by the Kolmogorov expression, as indeed confirmed in Fig. 8b.

5 Conclusions

The QNSE theory can be used to characterize seasonal oceanic variability on meso- and submesoscales in terms of the horizontal KE spectra. The theoretical expressions for the spectra are comprised of two terms describing the Kolmogorov and Coriolis branches. Being solely determined by the rate of the energy transfer, Π_ε, and the Coriolis parameter, f, they feature different spectral exponents. These bi-component spectra cannot be well approximated by a line with a single slope. Clearly, the importance of analyzing not only spectral slopes but also the amplitudes cannot be overstated. Besides, the amplitudes harbor substantial information about the physical processes governing the system. For example, in the framework of the dimensional analysis, it is often possible to infer a spectral slope from the variables forming the amplitude but the opposite is not true.

The theory predicts that the submesoscale processes can be quantified in terms of a single parameter, the energy flux Π_ε, that can be associated with the effective submesoscale dissipation, or ESD. This flux governs various submesoscale processes and may be quite different from the dissipation rate, ε, taking place on the microstructure. The analysis of oceanic observations shows that the values of Π_ε in winter may be higher than those in summer by up to an order of magnitude. This outcome is qualitatively consistent with other observational studies showing more energetic submesoscale dynamics in winter mixed layer compared to its summer counterpart in the northern

Table 2 Annual and seasonal values of L_t in the North-Western Pacific

Region	Latitude, ° N	Annual L_t	Seasonal L_t	
			Winter	Summer
Kuroshio	28–34	15	< 10	18
STCC	14–28	50	20	60
NEC	9–14	250	—-	—-
NECC	3-9	120	—-	—-

L_t is in km; the data is from Qiu et al. (2017)

hemisphere away from the tropics where the Kolmogorov subrange is substantial and turbulence exhibits a high level of intermittency. To the best of our knowledge, the seasonal oceanic variability on submesoscales has neither been quantified nor explained in terms of ESD in the preceding investigations.

The theory predicts higher variability on submesoscales than on mesoscales because the energy flux, Π_ε, is sensitive to seasonal energy flux changes due to instabilities, transients, fronts, and other factors. On the mesoscales, the variability is limited by the spectral amplitudes' dependence on the Coriolis parameter. These predictions are substantiated by comparisons of the theoretical and observed spectra in two seasons, winter and summer, at several locations in the North-West Atlantic and North-West Pacific Oceans.

Good agreement between the theoretical and observed spectra indicates that the theoretical expressions can be used to test the performance of numerical models. Such strategy has been used for atmospheric models as described, for instance, in Skamarock et al. (2014) where the ability of a numerical model to reproduce the Nastrom and Gage spectra has been often viewed as a measure of model's fidelity. In oceanographic research, steps are being made in a similar direction.

In addition, as was discussed in Section 3, the SGS schemes in the existing models may over-dissipate the KE. Comparisons of the computed and theoretical spectra have exposed the problem. The recent high-resolution simulations detailed in Nelson et al. (2020) demonstrate that the over-damping can be decreased with the increase in resolution as it diminishes the role of the SGS parameterization. The use of the QNSE-based SGS schemes may alleviate the over-damping problem in simulations with moderate resolution used in climate models.

The mesoscale range extends to large scales and features steeper spectra that harbor high values of the eddy KE. If the size of the eddies can be associated with the scale at which the mesoscale spectrum flattens out, as, for example, a scale around 100 km in Fig. 2 for the NEC, then the seasonal variability of the eddy KE can be estimated by integrating the Coriolis branch of (5).

As an illustration, this approach can be used to explain the relationship between the observed seasonal variability of the eddy size and the magnitude of the near-surface eddy KE in the tropical Atlantic ocean presented in Aguedjou et al. (2019). The data shows that in winter, the eddy size may reach 100 km while the eddy KE attains about 600 $cm^2\ s^{-2}$ while in summer, the scale reduces to about 70 km and the eddy KE drops to 300–400 $cm^2\ s^{-2}$. Taking into account that on such scales, the spectrum is approximately described by the Coriolis branch of (5) and integrating that equation for the specified parameters at $\theta \simeq 10°$, one recovers the observed values.

Acknowledgments This paper is partially based upon the presentation at the 11th International Workshop on Modeling the Ocean (IWMO2019) held in Wuxi, China, on June 17–20, 2019. Discussions with Leo Oey, Dong-Ping Wang, Fanghua Xu, Huijie Xue, Tal Ezer, Claude Cambon, Don Chambers, James Cho, Greg King, Stefania Espa, Simon Cabanes, Peter Read, Jinbo Wang, Dimitris Menemenlis and Lee-Lueng Fu are greatly appreciated.

Funding Partial funding was provided by the NASA/NOAA Ocean Surface Topography Science Team. BG received partial support through a University of South Florida Nexus Initiative (UNI) Award. SS received partial support from the Israel Science Foundation grant no. 408/15. BQ received support from NASA Grant NNX17AH33G.

Declarations

Conflict of interest The authors declare no competing interests.

References

McWilliams J (2019) A survey of submesoscale currents. Geosci Lett 6:3. https://doi.org/10.1186/s40562-019-0133-3

Yang Q, Nikurashin M, Sasaki H, Sun H, Tian J (2019) Dissipation of mesoscale eddies and its contribution to mixing in the northern South China Sea. Sci Rep 9:556. https://doi.org/10.1038/s41598-018-36610-x

Lindborg E (1999) Can the atmospheric kinetic energy spectrum be explained by two-dimensional turbulence? J Fluid Mech 388:259

Galperin B, Sukoriansky S (2020) Quasinormal scale elimination theory of the anisotropic energy spectra of atmospheric and oceanic turbulence. Phys Rev Fluids 5:063803. https://doi.org/10.1103/PhysRevFluids.5.063803

Zheng Q, Xie L, Xiong X, Hu X, Chen L (2020) Progress in research of submesoscale processes in the South China Sea. Acta Oceanol Sin 39:1. https://doi.org/10.1007/s13131-019-1521-4

Shcherbina A, Sundermeyer M, Kunze E, D'Asaro E, Badin G, Birch D, Brunner-Suzuki AME, Callies J, Cervantes BK, Claret M, Concannon B, Early J, Ferrari R, Goodman L, Harcourt R, Klymak J, Lee C, Lelong MP, Levine M, Lien RC, Mahadevan A, McWilliams J, Molemaker M, Mukherjee S, Nash J, Özgökmen T, Pierce S, Ramachandran S, Samelson R, Sanford T, Shearman RK, Skyllingstad E, Smith K, Tandon A, Taylor J, Terray E, Thomas L, Ledwell J (2015) The Latmix summer campaign. Bull Amer Meteorol Soc 96:1257

Callies J, Ferrari R, Klymak J, Gula J (2015) Seasonality in submesoscale turbulence. Nature Comm 6:6862. https://doi.org/10.1038/ncomms7862

Rocha C, Gille S, Chereskin T, Menemenlis D (2016) Seasonality of submesoscale dynamics in the Kuroshio Extension. Geophys Res Lett 43:11304. https://doi.org/10.1002/2016GL071349

Su Z, Wang J, Klein P, Thompson A, Menemenlis D (2018) Ocean submesoscales as a key component of the global heat budget, Nature Comm 9:775. https://doi.org/10.1038/s41467-018-02983-wDO

Qiu B, Chen S, Klein P, Wang J, Torres H, Fu LL, Menemenlis D (2018) Menemenlis, seasonality in transition scale from balanced to unbalanced motions in the world ocean. J Phys Oceanogr 48:591

Buckingham CE, Lucas NS, Belcher SE, Rippeth TP, Grant ALM, Sommer JL, Ajayi AO, Garabato ACN, Adv J (2019) The contribution of surface and submesoscale processes to turbulence in the open ocean surface boundary layer. Model Earth Syst 11:4066. https://doi.org/10.1029/2019MS001801

Li J, Dong J, Yang Q, Zhang X (2019) Spatial-temporal variability of submesoscale currents in the South China Sea. J Oceanol Limnol 37:474. https://doi.org/10.1007/s00343-019-8077-1

Zhang Z, Zhang Y, Qiu B, Sasaki H, Sun Z, Zhang X, Zhao W, Tian J, Geophys J (2020) Spatiotemporal characteristics and generation mechanisms of submesoscale currents in the northeastern South China Sea revealed by numerical simulations, vol 125. https://doi.org/10.1029/2019JC015404

Sasaki H, Klein P, Qiu B, Sasai Y (2014) Impact of oceanic-scale interactions on the seasonal modulation of ocean dynamics by the atmosphere. Nature Comm 5:5636. https://doi.org/10.1038/ncomms6636

Garrett C, Munk W (1979) Internal waves in the ocean. Annu Rev Fluid Mech 11:339

Garrett C (2006) Turbulent dispersion in the ocean. Progr Oceanogr 70:113

Sagaut P, Cambon C (2018) Homogeneous turbulence dynamics, 2nd edn. Springer, Berlin

Sukoriansky S, Galperin B, Staroselsky I (2005) A quasinormal scale elimination model of turbulent flows with stable stratification. Phys Fluids 17:085107

Sukoriansky S, Galperin B (2016) QNSE theory of turbulence anisotropization and onset of the inverse energy cascade by solid body rotation. J Fluid Mech 805:384. https://doi.org/10.1017/jfm.2016.568

Charney JG (1971) Geostrophic turbulence. J Atmos Sci 28:1087

Lindborg E (2006) The energy cascade in a strongly stratified fluid. J Fluid Mech 550:207

Lindborg E (2015) A Helmholtz decomposition of structure functions and spectra calculated from aircraft data. J Fluid Mech 762:R4

Vallgren A, Deusebio E, Lindborg E (2011) Possible explanation of the atmospheric kinetic and potential energy spectra. Phys Rev Lett 107:268501

Deusebio E, Vallgren A, Lindborg E (2013) The route to dissipation in strongly stratified and rotating flows. J Fluid Mech 720:66. https://doi.org/10.1017/jfm.2012.611

Dewan E (1979) Stratospheric wave spectra resembling turbulence. Science 204:832

VanZandt T (1982) A universal spectrum of buoyancy waves in the atmosphere. Geophys Res Lett 9:575

Callies J, Bühler O, Ferrari R (2016) The dynamics of mesoscale winds in the upper troposphere and lower stratosphere. J Atmos Sci 73:4853. https://doi.org/org/10.1175/JAS-D-16-0108.1

Lindborg E, Cho C (2001) Horizontal velocity structure functions in the upper troposphere and lower stratosphere 2. Theoretical considerations. J Geophys Res 106:10233

Skamarock W, Park SH, Klemp J, Snyder C (2014) Atmospheric kinetic energy spectra from global highresolution nonhydrostatic simulations. J Atmos Sci 71:4369

Blumen W (1978) Uniform potential vorticity flow: Part I. Theory of wave interactions and two-dimensional turbulence. J Atmos Sci 35:774. https://doi.org/10.1175/1520-0469(1978)035,0774:UPVFPI.2.0.CO;2

Juckes M (1994) Quasigeostrophic dynamics of the tropopause. J. Atmos. Sci. 51:2756. https://doi.org/10.1175/1520-0469(1994)051,2756:QDOTT.2.0.CO;2

Held I, Pierrehumbert R, Garner S, Swanson K (1995) Surface quasi-geostrophic dynamics. J Fluid Mech 282:1. https://doi.org/10.1017/S0022112095000012

Lapeyre G (2017) Surface quasi-geostrophy. Fluids 2:7. https://doi.org/10.3390/fluids2010007

Tulloch R, Smith K (2006) A theory for the atmospheric energy spectrum: Depth-limited temperature anomalies at the tropopause. Proc Natl Acad Sci USA 103:14690. https://doi.org/10.1073/pnas.0605494103

Tulloch R, Smith K (2009) Quasigeostrophic turbulence with explicit surface dynamics: Application to the atmospheric energy spectrum. J Atmos Sci 66:450. https://doi.org/10.1175/2008JAS2653.1

Lindborg E (2009) Two comments on the surface Quasigeostrophic model for the atmospheric energy spectrum. J Atmos Sci 66:1069. https://doi.org/10.1175/2008JAS2972.1

Smith K, Tulloch R (2009) Reply. J Atmos Sci 66:1073

Lovejoy S, Tuck A, Schertzer D, Hovde S (2009) Reinterpreting aircraft measurements in anisotropic scaling turbulence. Atmos Chem Phys 9:5007

Lindborg E, Tung K, Nastrom G, Cho J, Gage K (2009) Comment on "Reinterpreting aircraft measurement in anisotropic scaling turbulence" by Lovejoy et al. (2009). Atmos Chem Phys 9:22331

Lovejoy S (2009) Interactive comment on "Comment on "Reinterpreting aircraft measurements inanisotropic scaling turbulence" by Lovejoy etal. (2009)" by E. Lindborg et al. Atmos Chem Phys Discuss 9:C7688

Batchelor GK (1969) Computation of the energy spectrum in homogeneous two-dimensional turbulence. Phys Fluids 12:233

Kraichnan RH (1967) Inertial ranges in two-dimensional turbulence. Phys Fluids 10:1417

Leith C (1968) Diffusion approximation for two-dimensional turbulence. Phys Fluids 11:671

Bierdel L, Snyder C, Park SH, Skamarock W (2016) Accuracy of rotational and divergent kinetic energy spectra diagnosed from flight-track winds. J Atmos Sci 73:3273

Asselin O, Bartello P, Straub D (2018) On Boussinesq dynamics near the tropopause. J Atmos Sci 75:571

Yano JI (2010) Interactive comment on "Why anisotropic turbulence matters: another reply" by S. Lovejoy et al. Atmos Chem Phys Discuss 10:C1625

Yakhot V, Orszag S (1986) Renormalization group analysis of turbulence. I. Basic theory. J Sci Comput 1:3

Celani A, Musacchio S, Vincenzi D (2010) Turbulence in more than two and less than three dimensions. Phys Rev Lett 104:184506

Ecke R (2017) From 2D to 3D in fluid turbulence: unexpected critical transitions. J Fluid Mech 828:1. https://doi.org/10.1017/jfm.2017.507

Deusebio E, Boffetta G, Lindborg E, Musacchio S (2014) Dimensional transition in rotating turbulence. Phys Rev E 023005:90

Qiu B, Chen S, Klein P, Sasaki H, Sasai Y (2014) Seasonal mesoscale and submesoscale eddy variability along the North Pacific subtropical countercurrent. J Phys Oceanogr 44:3079. https://doi.org/10.1175/JPO-D-14-0071.1

Pouquet A, Marino R, Mininni P, Rosenberg D (2017) Dual constant-flux energy cascades to both large scales and small scales. Phys Fluids 111108:29

King GP, Vogelzang J, Stoffelen A, Geophys J (2015) Upscale and downscale energy transfer over the tropical Pacific revealed by scatterometer winds. Res Oceans 120:346. https://doi.org/10.1002/2014JC009993

Sahoo G, Alexakis A, Biferale L (2017) Discontinous transitions from direct to inverse cascade in threedimensional turbulence. Phys Rev Lett 164501:118

Byrne D, Zhang J (2013) Height-dependent transition from 3-D to 2-D turbulence in the hurricane boundary layer. Geophys Res Lett 40:1439. https://doi.org/10.1002/grl.50335, 2013

Qiu B, Nakano T, Chen S, Klein P (2017) Submesoscale transition from geostrophic flows to internal waves in the northwestern Pacific upper ocean. Nature Comm 8:14055

Nastrom G, Gage K, Jasperson W (1984) Kinetic energy spectrum of large- and mesoscale atmospheric processes. Nature 310:36

Monin A, Yaglom A (1975) Statistical fluid mechanics. MIT Press, Cambridge

Kimura Y, Herring JR (2012) Energy spectra of stably stratified turbulence. J Fluid Mech 698:19. https://doi.org/10.1017/jfm.2011.546

Schubert R, Gula J, Greatbatch RJ, Baschek B, Biastoch A (2020) The submesoscale kinetic energy cascade: mesoscale absorption of submesoscale mixed layer eddies and frontal downscale fluxes. J Phys Ocean 50(9):2573. https://doi.org/10.1175/JPO-D-19-0311.1

Rocha C, Chereskin T, Gille S, Menemenlis D (2016) Menemenlis, mesoscale to submesoscale wavenumber spectra in Drake passage. J Phys Oceanogr 46:601

Wang S, Liu Z, Pang C (2015) Geographical distribution and anisotropy of the inverse kinetic energy cascade, and its role in the eddy equilibrium processes. J Geophys Res Oceans 120:4891. https://doi.org/10.1002/2014JC010476

Bradshaw P (1973) Effects of streamline curvature on turbulent flow. AGARDograph 169

Poje A, Özgökmen T, Bogucki D, Kirwan A (2017) Kirwan, Evidence of a forward energy cascade and Kolmogorov self-similarity in submesoscale ocean surface drifter observations. Phys Fluids 020701:29

D'Asaro E, Lee C, Rainville L, Harcourt R, Thomas L (2011) Enhanced turbulence and energy dissipation at ocean fronts. Science 332:318

Zhang Z, Tian J, Qiu B, Zhao W, Chang P, Wu D, Wan X (2016) Observed 3D structure, generation, and dissipation of oceanic mesoscale eddies in the South China Sea. Sci Reports 6:24349. https://doi.org/10.1038/srep24349

Gula J, Molemaker M, McWilliams J (2016) Topographic generation of submesoscale centrifugal instability and energy dissipation. Nature Comm 7:12811. https://doi.org/10.1038/ncomms12811

Golitsyn G (2018) Random walk laws by A.N. Kolmogorov as the basics for understanding most phenomena of the Nature. Izv Atm Ocean Phys 54:223

Galperin B, Sukoriansky S (2010) Geophysical flows with anisotropic turbulence and dispersive waves: flows with stable stratification. Ocean Dyn 60:1319. https://doi.org/10.1007/s10236-010-0325-z

Sukoriansky S, Galperin B (2013) An analytical theory of the buoyancy - Kolmogorov subrange transition in turbulent flows with stable stratification. Philos Trans Royal Soc A 371:20120212. https://doi.org/10.1098/rsta.2012.0212

Dritschel D, McIntyre M (2008) Multiple jets as PV staircases: The Phillips effect and the resilience of eddytransport barriers . J Atmos Sci 65:855

McIntyre M (2008) Potential-vorticity inversion and the wave-turbulence jigsaw: some recent clarifications. Adv Geosci 15:47

Wood R, McIntyre M (2010) A general theorem on angular-momentum changes due to potential vorticity mixing and on potential-energy changes due to buoyancy mixing. J Atmos Sci 67:1261

Galperin B, Hoemann J, Espa S, Di Nitto G (2014) Anisotropic turbulence and Rossby waves in an easterly jet - An experimental study. Geophys Res Lett 41:6237. https://doi.org/10.1002/2014GL060767

Shcherbina AY, D'Asaro EA, Lee CM, Klymak J, Molemaker MJ, McWilliams J (2013) Statistics of vertical vorticity, divergence, and strain in a developed submesoscale turbulence field. Geophys Res Lett 40:4706. https://doi.org/10.1002/grl.50919

Wang DP, Flagg C, Donohue K, Rossby H (2010) Wavenumber spectrum in the Gulf Stream from shipboard ADCP observations and comparison with altimetry measurements. J Phys Oceanogr 40:840. https://doi.org/10.1175/2009JPO4330.1

Bühler O, Kuang M, Tabak E (2017) Anisotropic Helmholtz and wave-vortex decomposition of onedimensional spectra. J Fluid Mech 815:361

Dong J, Fox-Kemper B, Zhang H, Dong C (2020) The seasonality of submesoscale energy production, content, and cascade, vol 47. https://doi.org/10.1029/2020GL087388

Chelton DB, Schlax MG (1996) Global observations of oceanic rossby waves. Science 272:234. https://doi.org/10.1126/science.272.5259.234

Galperin B, Read PL (eds) (2019) Zonal Jets: Phenomenology, genesis and physics. Cambridge University Press, Cambridge. https://doi.org/10.1017/9781107358225.014

Nelson A, Arbic B, Menemenlis D, Peltier W, Alford M, Grisouard N, Klymak J, Geophys J (2020) Improved internal wave spectral continuum in a regional ocean model. Res. Oceans 125:e2019JC015974. https://doi.org/10.1029/2019JC015974

Aguedjou H, Dadou I, Chaigneau A, Morel Y, Alory G (2019) Eddies in the Tropical Atlantic Ocean and their seasonal variability. Geophys Res Lett 46(12):156. https://doi.org/10.1029/2019GL083925